SP STYLE AND FORMAT GUIDELINES

Papers accepted for publication in an ACI SP should not exceed 20 single-spaced pages. Each manuscript must include the following:

- **Title of paper** – The title should not exceed 70 characters.

- **Brief abstract or synopsis** – The abstract/synopsis should not exceed 200 words and should contain the essential results and conclusions.

- **Keywords** – A maximum of nine (9) keywords is suggested. Print the word "Keywords" followed by a colon at the left margin at the bottom of the first page and insert keywords in alphabetical order.

- **Brief author biography** – The author biography should not exceed 75 words.

- **Dual units** – Either SI (metric) or inch-pound units of measurement can be used as primary units, and the secondary units must be provided in parentheses. Papers are not published without dual units. A metrication conversion guide is available here:

  http://www.concrete.org/Portals/0/Files/Excel/MetricationGuide.xls

An example manuscript is included at the end of these guidelines.

Order of Elements

First page: The first page of the manuscript is reserved for the title, author name(s), synopsis, and keywords. Please center the paper title and authors' names at the top of the page. Leave three lines blank, print the word "Synopsis" followed by a colon at the left margin, and then key in the synopsis. Keywords should follow at the bottom of the page.

Last page: Include a brief biographical sketch of each author at the end of the manuscript. Please limit each biography to five lines and include one blank line between each listing. Single space all text with a double space between paragraphs.

Other Guidelines

Basic format: All margins must be one inch (1") on each side. Text must be single spaced, 10-point, Times New Roman font.

Headings: Major headings, e.g., INTRODUCTION, METHODS, RESULTS, etc. should be printed in all capital letters and centered on the page. Subheads should be underlined, flush with the left margin, and with only the first letter capitalized. Third level headings should be underlined, indented, the first letter capitalized, and run into the text using an em-dash (—) to separate it from the text.

SP STYLE AND FORMAT GUIDELINES

Brand names: Brand names, product names, and/or company names should not be in SP papers.

References: References should be indicated in the text by consecutive superscript numbers or should be in author/date format. Each full reference should be listed in a reference section at the end of the paper. (See Chapter 8 of the *Technical Committee Manual (TCM)* for details.)

Tables: Tables should be developed using Microsoft Word® and placed within the text of the SP or grouped together in sequential order, following the references. Do not develop tables in Microsoft Excel®. All tables should be numbered and have headings.

Figures: Figures should be placed within the text of the SP or grouped together in sequential order, following the tables. All figures should be numbered, with captions printed directly below the appropriate figures. The photo resolution should be 300 dpi or higher for optimum print quality.

Captions: Captions for tables and figures should be consistent. ACI recommends that authors include the table or figure number followed by an em-dash (—) and the caption information. For example:
Figure 1—Crack patterns for S1 and S2.

Additional Style Guidelines:

- Consistently use automatic word wrap (soft returns) for sentences within a paragraph, and the Enter or Return key (hard return) at the end of a paragraph.

- Except for paragraphs, do not use tabs in the text (i.e., do not indent blocks of text).

- Refrain from using text boxes. No figures, tables, captions, or text should be put in text boxes.

- Refrain from using hairlines in graphs (line widths below 0.5 pt).

- Use the numeral 1, not the lower case "ell" for the number one.

- Use the numeral 0, not the capital "oh" for zero.

- Use consistent spacing throughout the document.

- Use the word processor's automatic footnote capability.

Response Surface Metamodel-based Performance Reliability for Reinforced Concrete Beams Strengthened with FRP sheets

Junwon Seo, Yail J. Kim, and Shadi Zandyavari

Synopsis: This paper presents the performance reliability of reinforced concrete beams strengthened with fiber reinforced polymer (FRP) sheets, including structural fragility. Emphasis is placed on the development of effective strains that can represent FRP-debonding failure. The reliability predicted by a conventional standard log-normal cumulative probability density function and by the proposed response surface metamodel (RSM) combined with Monte-Carlo simulation (MCS) is employed to assess the contribution of physical attributes to debonding failure. The models are constructed based on a large set of experimental database consisting of 230 test beams collected from published literature. Another aspect of the study encompasses the effect of various RSM parameters on the variation of effective strains, such as FRP thickness (t_f), steel reinforcement ratio (ρ), concrete strength (f'_c), beam height (h), beam width (w), span length (L), and shear span (a). The mutual interaction between these parameters indicates that those related to beam geometry (i.e., L, w, h, and a parameters) and the t_f parameter are significant factors influencing the effective strain of FRP-strengthened beams.

Seo et al.

ACI member **Junwon Seo** is an Assistant Professor in the Department of Civil and Environmental Engineering at South Dakota State University, Brookings, SD. He is an associate member of ACI Committees 341 (Earthquake-Resistant Concrete Bridges), 343 (Concrete Bridge Design: Joint ACI-ASCE), and 345 (Concrete Bridge Construction, Maintenance, and Repair). His research interests encompass the structural behavior of irregular bridges and other structures, multi-hazard vulnerability and sustainability assessment, repair, retrofit and rehabilitation, structural reliability and risk analysis, and structural health monitoring. He is a licensed Professional Engineer in Iowa.

ACI member **Yail J. Kim** is an Associate Professor in the Department of Civil Engineering at the University of Colorado Denver, Denver, CO. He is the Chair of ACI Committee 345 (Concrete Bridge Construction, Maintenance, and Repair) and is a member of Committees 342 (Evaluation of Concrete Bridges and Bridge Elements) and 440 (Fiber Reinforced Polymer Reinforcement). He also chairs ACI 440I (FRP-prestressed Concrete). His research interest includes the application of advanced composite materials for structures, structural complexity, structural reliability, and science-based structural engineering, including and statistical and quantum physics. He is a licensed Professional Engineer in the Province of Ontario, Canada.

ACI student member **Shadi Zandyavari** is a Graduate Student in the Department of Civil and Environmental Engineering at South Dakota State University, Brookings, SD.

INTRODUCTION

Structural fragility/reliability has been used for assessing seismic risk in constructed facilities such as highway bridges. Fragility (also known as vulnerability) is defined as a conditional probability that a structure exceeds a prescribed damage state when subjected to various levels of natural or man-made hazards. Reliability is, on the other hand, defined as the extent of achieving the given functionality of a structure exposed to distressful hazards. Previous studies have shown that use of either empirical or analytical vulnerability functions can be regarded as one of the standard approaches for seismic fragility estimation [1-9], while analytical vulnerability functions are dominantly employed because in-situ data are limitedly available in most cases [1-6]. Conventional methodologies for generating analytical vulnerability functions include the statistical extrapolation of a structure's performance along with Monte Carlo simulation (MCS) [2-6]. Seo et al. [5] estimated the structural fragility of steel moment-frame structures using MCS-based response surface metamodels (RSM). The joint RSM-MCS method enables the efficient fragility assessments of a group of steel moment-frame structures when compared to the conventional methodologies. Ghosh et al. [6] utilized metamodels combined with MCS to evaluate existing bridges subjected to seismic load. Although the concept of structural fragility and corresponding reliability are proven to be robust in evaluating the performance of civil structures, it has not fully been integrated into the resiliency appraisal of retrofitted structural members.

Over the past couple of decades, fiber reinforced polymer (FRP) composites have been used for enhancing the behavior of deteriorated reinforced concrete members, including several advantages such as favorable strength-to-weight ratio, non-corrosive characteristics, and reduced long-term maintenance costs [10]. A number of studies on FRP-strengthening were concerned with the performance evaluation of various structural systems in static, fatigue, and seismic loadings [11]. The reliability-oriented assessment of such a strengthening method was, however, rarely reported, particularly structural fragility accounting for critical failure modes such as FRP-debonding. This paper proposes a theoretical framework for examining the debonding vulnerability of reinforced concrete beams strengthened with FRP sheets. Of interest is a relationship between FRP-debonding and performance reliability. An RSM model was built using a large number of laboratory test data compiled from published literature, encompassing geometric and material parameters, in order to predict the effective strain of FRP. It is worth noting that the effective strain controls the response of a strengthened beam in such a way that FRP-debonding failure takes place when the strain of the strengthening system exceeds its effective strain. The experimentally validated RSM model coupled with MCS was implemented to generate the debonding fragility of FRP-strengthened beams, which was compared with a conventional fragility approach, followed by quantifying performance reliability.

2

RESPONSE SURFACE METAMODEL

This section discusses the development of a prediction model for debonding strain of an FRP-strengthened beam based on a statistical approach and its validation against experimental data.

Development

The RSM model proposed is a second-order polynomial function as shown in Eq. 1:

$$y = \beta_0 + \sum_{i=1}^{k}\beta_i x_i + \sum_{i=1}^{k}\beta_{ii}x_i^2 + \sum_{i=1}^{k=1}\sum_{j>i}^{k}\beta_{ij}x_i x_j + \varepsilon \tag{1}$$

where y is the dependent variable representing the effective FRP strain of a strengthened beam at debonding failure; x_i and x_j are the independent input variables dependent upon the geometric and material properties of the beam; β_0, β_i, β_{ii}, and β_{ij} are empirical coefficients to be determined by statistical analysis on test data; k is the number of input variables, and ε is the statistical bias. Such a statistical RSM model is expected to generate a fragility curve for FRP-strengthened members at low computational expenses [5]. A large set of database comprising 230 test beams was used to develop an RSM model, as listed in Table 1 where several parameters are presented: beam height (h), beam width (w), span length (L), shear span (a), compressive strength of concrete (f'_c), thickness of FRP (t_f), and steel reinforcement ratio (ρ). The effect of shear span (a) and shear-span-to-depth-ratio (a/d) on the flexure of the beams is basically identical from a fundamental mechanics standpoint. To identify the necessary statistical coefficients of the parameterized model, the JMP software [12] was utilized for least-square analysis. Equation 2 is the refined format of the proposed RSM model (units are in mm and MPa) to predict the effective stain of an FRP-strengthened beam (ε_e):

$$\begin{aligned}
\varepsilon_e = {} & \beta_0 + \beta_1(L - L_{ave}) + \beta_2(w - w_{ave}) + \beta_3(h - h_{ave}) + \beta_4(\rho - \rho_{ave}) + \beta_5(a - a_{ave}) + \beta_6\left(\sqrt{f'_c} - \sqrt{f'_{c\,ave}}\right) \\
& + \beta_7\left(\sqrt{t_f} - \sqrt{t_{f\,ave}}\right) + \beta_8(L - L_{ave})^2 + \beta_9(L - L_{ave})(w - w_{ave}) + \beta_{10}(L - L_{ave})(h - h_{ave}) + \beta_{11}(L - L_{ave})(\rho - \rho_{ave}) \\
& + \beta_{12}(L - L_{ave})(a - a_{ave}) + \beta_{13}(L - L_{ave})\left(\sqrt{f'_c} - \sqrt{f'_{c\,ave}}\right) + \beta_{14}(L - L_{ave})\left(\sqrt{t_f} - \sqrt{t_{f\,ave}}\right) + \beta_{15}(w - w_{ave})^2 \\
& + \beta_{16}(w - w_{ave})(h - h_{ave}) + \beta_{17}(w - w_{ave})\rho + \beta_{18}(w - w_{ave})(a - a_{ave}) + \beta_{19}(w - w_{ave})\left(\sqrt{f'_c} - \sqrt{f'_{c\,ave}}\right) \\
& + \beta_{20}(w - w_{ave})\left(\sqrt{t_f} - \sqrt{t_{f\,ave}}\right) + \beta_{21}(h - h_{ave})^2 + \beta_{22}(h - h_{ave})(\rho - \rho_{ave}) + \beta_{23}(h - h_{ave})(a - a_{ave}) \\
& + \beta_{24}(h - h_{ave})\left(\sqrt{f'_c} - \sqrt{f'_{c\,ave}}\right) + \beta_{25}(h - h_{ave})\left(\sqrt{t_f} - \sqrt{t_{f\,ave}}\right) + \beta_{26}(\rho - \rho_{ave})^2 + \beta_{27}(\rho - \rho_{ave})(a - a_{ave}) \\
& + \beta_{28}(\rho - \rho_{ave})\left(\sqrt{f'_c} - \sqrt{f'_{c\,ave}}\right) + \beta_{29}\rho\left(\sqrt{t_f} - \sqrt{t_{f\,ave}}\right) + \beta_{30}(a - a_{ave})^2 + \beta_{31}(a - a_{ave})\left(\sqrt{f'_c} - \sqrt{f'_{c\,ave}}\right) \\
& + \beta_{32}(a - a_{ave})\left(\sqrt{f'_c} - \sqrt{f'_{c\,ave}}\right) + \beta_{33}\left(\sqrt{f'_c} - \sqrt{f'_{c\,ave}}\right)^2 + \beta_{34}\left(\sqrt{f'_c} - \sqrt{f'_{c\,ave}}\right) + \beta_{35}\left(\sqrt{t_f} - \sqrt{t_{f\,ave}}\right)^2
\end{aligned} \tag{2}$$

Table 2 exhibits the average properties of each RSM parameter, while Table 3 summarizes the statistically determined RSM coefficients (β_0 through β_{35}).

Validation

Figure 1 shows a typical comparison between the experimental and predicted debonding strains (or effective strains) with respect to FRP thickness. With an increase in FRP thickness (t_f), the effective strain of the strengthened beams was exponentially reduced. This observation can be explained by the fact that interfacial shear stresses along the bond-line of the beams augmented when an FRP thickness increased until the stress exceeded a critical stress that would result in FRP-debonding failure. Acceptable agreement was made between the test and model, as shown in Fig. 1, with a correlation coefficient of 0.75. The margins of error for the predicted mean and standard deviation against those of the test data were 36% and 26%, respectively. Given that the experimental beams were independently designed and tested by a number of researchers, such a range of prediction error appears to be inevitable [13]. Although some discrepancy was noticed between the test and prediction, it is reasonable to conclude that the RSM model developed can represent the behavior of FRP-strengthened beams in terms of effective strains.

EFFECT OF PARAMETER VARIATION

The effect of the aforementioned RSM parameters and the mutual interaction between two selected attributes and FRP-debonding were studied in the following subsections.

Effect of a Single Parameter

Figure 2 shows the variation of effective strains with respect to the RSM parameters, including FRP thickness (t_f), steel reinforcement ratio (ρ), concrete strength (f'_c), beam height (h), beam width (w), span length (L), and shear span (a). It was found that the effective strain of FRP tended to decrease with an increase in the h, L, ρ, and t_f parameters, while tended to increase when the w, f'_c, and a parameters were raised. The physical interpretation of each attribute is discussed as follows:

- *FRP thickness* [Fig. 2(a)]: as explained previously, FRP thickness influences the development of interfacial stress along the bond-line. From a mechanics point of view, the interfacial stress is a function of hyperbolic trigonometry with respect to FRP thickness [14]
- *Steel reinforcement ratio* [Fig. 2(b)]: when more steel reinforcing bars are used the flexural rigidity of the beam augments (i.e., the stiffness of the beam increases), thereby accelerating the development of normal stresses along the bonded FRP. It should, however, be noted that such an increase in flexural rigidity may not be significant, which is in conformance with the variation range of the effective strain given in Fig. 2(b)
- *Concrete strength* [Fig. 2(c)]: FRP-debonding occurs inside a concrete substrate in most cases since the strength of the concrete cover is less than that of a bonding agent. An increase in concrete strength can, therefore, increase resistance to the occurrence of FRP-debonding
- *Beam height* [Fig. 2(d)]: the effect of beam height is in principle analogous to that of the steel reinforcement ratio, provided that an increase in beam height results in an increase in flexural rigidity
- *Beam width* [Fig. 2(e)]: as the width of a beam soffit becomes wider, interfacial stresses are reduced due to an increased contact area. The full coverage of a beam substrate by FRP is thus generally recommended in practice
- *Beam length* [Fig. 2(f)]: the bending moment of a beam is directly proportional to its span length so that any increase in flexural moment detrimentally affects the behavior of the strengthened beam, which entails an increased probability of FRP-debonding.
- *Shear span* [Fig. 2(g)]: the applied shear stress to the interfacial layer is redistributed when the length of a shear span increased, which is similar to the stress-reduction mechanism discussed in the beam width parameter.

According to the RSM prediction (Fig. 2), significant parameters influencing the effective strain of a strengthened beam were FRP thickness, beam width, beam length, and shear span. Given the geometric properties of an existing beam may not be controllable when a strengthening design is conducted, attention should be paid to the thickness of FRP: if thick FRP sheets are necessary to meet the requirement of flexural strengthening, additional thoughts shall be necessary such as use of anchorage for addressing premature debonding failure, in addition to a debonding strain check as per design guidelines. Table 4 lists the results of multivariate analysis of variance (MANOVA), including F statistics for individual parameters. All parameters were statistically meaningful at a confidence level of 95% except for the beam height (h) and steel reinforcement ratio (ρ). The most influential factor was the FRP thickness ($\sqrt{t_f}$), followed by the beam width (w) and concrete strength ($\sqrt{f'_c}$). These observations statistically confirm the contributing parameters of mechanics-based FRP-debonding models [14], namely, the occurrence of debonding failure is dominated by the extent of interfacial stresses that are a function of FRP thickness and bonded area as well as the substrate concrete strength.

Interaction between Two Parameters

Figures 3 to 8 exhibit the mutual interaction between the RSM parameters influencing the effective strain of FRP-strengthened beams. The variation range of each parameter was taken from the maximum and minimum values of those listed in Table 1. When two parameters were simultaneously compared, all other parameters mentioned earlier were set to their average values (Table 2). The interaction effect of beam height (h) along with other parameters is provided in Fig. 3. It was found that a combination of the beam height (h) and beam length (L) parameters had the most significant impact on the variation of effective strains ranging from 0% to 3.5% [Fig. 3(b)], while that of the beam height (h) and steel reinforcement ratio (ρ) was least influential on the effective strain development from 0% to 0.8% [Fig. 3(c)]. It should be worthwhile to note that the efficacy of FRP-strengthening is virtually none when the

effective strain value of 0% is associated. Figure 4 is dedicated to the contribution of the beam width parameter (w). The interaction between the beam width (w) and beam length (L) parameters was noticeable [Fig. 4(a)], given a large variation in effective strain was predicted up to 7%. A combination between the beam length (L) and FRP thickness (t_f) parameters resulted in a substantial effect on developing effective strains from 0% to 8% when compared to other cases, as shown in Fig. 5. The interaction effect of steel reinforcement ratio (ρ) is given in Fig. 6. The effective strain of FRP-strengthened beams changed from 0.3% to 0.7% when the concrete strength (f'_c) parameter increased from 20 MPa to 80 MPa at a reinforcement ratio of 0.5% [Fig. 6(a)]; on the other hand, the variation range of the effective strain enlarged as the reinforcement ratio (ρ) approached 4% where effective strains varied from 0% to 0.8%. As shown in Fig. 6(b), a simultaneous increase in steel reinforcement ratio (ρ) and FRP thickness (t_f) caused a consistent decrease in effective strain. Although a high reinforcement ratio tended to reduce the effectiveness of FRP-strengthening (i.e., low effective strain), such a trend became compensated with an increase in shear span length [Fig. 6(c)] due to the stress redistribution mechanism explained earlier. Figure 7(a) illustrates that the shear span parameter (a) was much more susceptible to the development of effective strain than concrete strength (f'_c). The contribution of the FRP thickness (t_f) and shear span (a) parameters was however similar, as shown in Fig. 7(b). The last interaction effect was provided in Fig. 8, including the concrete strength (f'_c) and FRP thickness (t_f) parameters. When an FRP thickness increased from 0 mm [0 in] to 5 mm [0.2 in] at a concrete strength of 20 MPa [2900 psi], the effective strain was reduced from 0.3% to 0%. Such a change in effective strain became more pronounced as a concrete strength augmented. For instance, the effective strain decreased from 0.9% to 0.2% and 1.3% to 0.4% with a variation in FRP thickness from 0 mm [0 in] to 5 mm [0.2 in] at a concrete strength of 50 MPa [7250 psi] and 80 MPa [11600 psi], respectively. It should be noted that an FRP thickness of 0 mm [0 in] given in Fig. 8 can indicate a very thin thickness of FRP sheet (e.g., t_f = 0.167 mm [0.0066 in], [15]), rather than an unstrengthened case.

FRAGILITY OF FRP-DEBONDING AND PERFORMANCE RELIABILITY

The structural fragility of FRP-debonding associated with performance reliability was predicted using a conventional standard log-normal cumulative probability density function and the joint RSM-MCS method. Below is a summary of the modeling approaches taken and technical discussion.

Model Formulation
Conventional fragility approach
The probability of debonding occurrence may be predicted by Eq. 3 [16]:

$$p_f = \Phi\left[\frac{\ln(S_d/S_c)}{\sqrt{\beta_d^2 + \beta_c^2}}\right] \tag{3}$$

where $\Phi[\ ]$, S_d, S_c, β_d, and β_c are the standard normal distribution function, the demand of FRP-debonding, the median capacity of FRP-concrete interface, and corresponding logarithmic standard deviations, respectively. The demand of FRP-debonding may be expressed by [16]:

$$S_d = x^a e^b \tag{4}$$

where x is the RSM parameter and a and b are the regression coefficients of the FRP-effective strain (ε_e) which can be obtainable from Eqs. 2 and 5:

$$\ln(\varepsilon_e) = a\ln(x) + b \tag{5}$$

To generate a conventional FRP-debonding fragility curve, the experimental effective strains corresponding to the metrics listed in Table 1 was used to calculate the probability of exceedance related to the constituent parameters. Figure 9(a) typically shows how to obtain the regression coefficients a and b using a relationship between the effective strain and beam width. The slope and intercept of the best-fit line provided the following coefficients: a = 0.1804 and b = -1.5628. The demand of FRP-debonding (S_d) and its standard deviation (β_d) were then computed for each beam width of the 230 experimental beams listed in Table 1. The median capacity of the FRP-concrete

Seo et al.

interface (S_c) and corresponding standard deviation (β_c) were estimated for the 230 beam data using the equation proposed by Kim and Harries [17]:

$$\varepsilon_e = \frac{0.05}{100} \left(\frac{wa}{hL\rho} \right)^{0.1} \sqrt{\frac{f_c'}{t_f}}$$

(6)

in which all the variables are defined earlier and their units are in mm and MPa. The solved results were substituted into Eq. 3 to determine the exceedance probability of a specific value for all the parameters associated with FRP-debonding (Eq. 2). Finally, the performance reliability (R_p) of an FRP-strengthened beam in terms of debonding resistance is obtained:

$$R_p = 1 - p_f$$

(7)

Joint RSM-MCS fragility
Best-fit distribution functions for each parameter given in Table 1 were acquired using the *allfitdist* feature of the MATLAB software [18] that can fit various types of probability distributions within an empirical distribution range. The fitted distribution functions were linked with MCS for numerical iteration assisted by the Cristal Ball software [19]. Two kinds of parameters were taken into consideration: governing and non-governing parameters. The value of a governing parameter was fixed, whereas that of a non-governing parameter was randomly selected within a boundary of the fitted distribution function. For example, FRP thickness has a substantial variation within the given interval [Fig. 2(a)] so that this attribute can be considered a governing parameter. The rest of non-governing parameters, including steel reinforcement ratio, beam height, beam width, beam length, concrete strength, and shear span, are sampled in random order from their intervals at a certain FRP thickness for the generation of an FRP variation-based fragility curve. The effective strains generated by the MCS (10,000 random samples per parameter) were compared with those predicted by Eq. 6 so that the probability of exceedance could be estimated for a specific governing parameter. A value in a fragility curve is then created for a certain failure level in conjunction with effective strains. Such a process is repeated at other failure levels to generate a fragility curve for different failure levels of another governing parameter. Lognormal functions were also fitted to the simulated data of each parameter. For example, Fig. 9(b) reveals an example plot for the beam width parameter with respect to effective strains. The intercept and slope of the fitted line on a lognormal distribution response were taken as the mean and standard deviation of the logarithmic relationship between the effective strain and beam width and were used for developing an MCS fragility curve.

Predicted Performance Reliability
Figure 10 shows the predicted performance reliability of each RSM parameter, along with a comparison between the conventional and RSM-MSC approaches. Figure 10(a) emphasizes the effect of FRP thickness. The reliability of the FRP-concrete interface estimated by the conventional method at an FRP thickness of 1 mm, 2 mm, 4 mm, and 6 mm was 60%, 25%, 12%, and 7%,,, respectively, while corresponding RSM-MSC solutions provided 58%, 25%, 18%, and 15%. This appears that there is no significant discrepancy at all values of the FRP thickness between these two approaches. The contribution of a steel reinforcement ratio to performance reliability was not substantial unlike the case of the FRP thickness parameter, as shown in Fig. 10(b) where a variation range between 60% and 40% was predicted. Given a steel reinforcement ratio less than 2% is typically used in practice, the performance reliability of strengthened beams may be regarded as 50% irrespective of the steel ratio. Figure 10(c) illustrates a relationship between the reliability and concrete strength. When the concrete strength of the strengthened beam was less than 30 MPa [4350 psi], the reliability was maintained below 30%. Such a low level of reliability, however, gradually increased with an increase in concrete strength. These observations imply that aged concrete structures with a low concrete strength (e.g., 20 MPa [2900 psi] or less) may need extra care when a strengthening design is carried out. Figures 10(d) through (g) depict the effect of beam geometry on the variation of reliability. The contribution of the beam length parameter [Fig. 10(f)] was relatively less significant than that of other parameters. The significant discrepancy between the conventional and the RSM-MSC methods shown in Fig. 10(f) is attributed to the fact that the slope and intercept of the best-fit line created by the conventional method, using the effective strains corresponding to discrete points of beam length from the limited experimental database, are not identical to those created by the RSM-MCS with the corresponding effective strains that were replicated via the RSM.

6

SUMMARY AND CONCLUDING REMARKS

This study has examined performance reliability associated with the structural fragility of FRP-strengthened beams (i.e., effective strain) based on a conventional standard log-normal cumulative probability density function and the proposed joint RSM-MCS method. A large set of 230 experimental data was employed to develop an RSM function for FRP-strengthened beams and the response of unstrengthened beams was outside the scope of the research. The effect of various geometric configurations, that is to say a size effect, was examined when interacting with other physical attributes. The conventional and the proposed approaches exhibited nearly indistinguishable responses for most parameters, excluding the beam length parameter, and hence further refinement appears to be necessary to claim the effectiveness of the proposed approach. Nevertheless, an ultimate merit of the application of joint RSM-MCS to the experimental beam data is its flexibility for efficient use in their performance reliability and parametric studies to examine the single effect and mutual interaction between RSM parameters. Specifically, studied was the mutual interaction between the RSM parameters and FRP-debonding. The effective strain of the FRP-concrete interface was influenced by a number of attributes such as stress redistribution along the bond-line, flexural rigidity of the strengthened beam, failure plane, and external loading conditions. With an increase in the beam height and length, steel reinforcement ratio, and FRP thickness parameters, the effective strains were reduced; however, the effect of the beam width, concrete strength, and shear span parameters showed an opposite trend. The mutual interaction between the RSM parameters revealed that the beam geometry (i.e., length, width, height, and shear span) and FRP thickness were significant factors affecting the effective strain development. The contribution of concrete strength was somewhat notable, while that of a reinforcement ratio was negligible. The degree of surface preparation for a concrete substrate could be another parameter to consider, whereas most published papers did not provide quantifiable information which restricted a mathematical formulation in the current investigation. The predicted performance reliability illustrated that the risk of FRP-debonding failure was substantially raised when an FRP thickness increased and when a low concrete strength was used.

ACKNOWLEDGMENTS

REFERENCES

[1] Shirazian, S., Ghayamghmian, M.R., and Nouri, G.R., 2011, "Developing of fragility curve for two-span simply supported concrete bridge in near fault area", World of Science, Engineering and Technology Conference, 51, 450-454.

[2] Unnikrishnan, V.U., Prasad, M.A., and Rao, B.N., 2013, "Development of fragility curves using high dimensional model representation", Journal of Earthquake Engineering and Structural Dynamics, 42, 419-430.

[3] Seo, J. and Linzell, D.G., 2010, "Probabilistic vulnerability scenarios for horizontally curved, steel, I-girder bridges under earthquake loads", Journal of Transportation Research Board, 2202(3), 206-211.

[4] Seo, J., and Linzell, D.G., 2012, "Horizontally curved steel bridge seismic vulnerability assessment", Engineering Structures, 34, 21-32.

[5] Seo, J., Duenas-Osorio, L., Craig, J.I., and Goodno, B.J., 2012, "Metamotel-based regional vulnerability estimate of irregular steel moment-frame structures subjected to earthquake events", Engineering Structures, 45, 585-597.

[6] Ghosh, J., Padgett, J.E., and Duenas-Osorio, L., 2013, "Surrogate modeling and failure surface visualization for efficient seismic vulnerability assessment of highway bridges", Journal of Probabilistic Engineering Mechanics, 34, 189-199.

[7] Gulec, C.K., Whittaker, A.S., and Hooper, J.D., 2010, "Fragility functions for low aspect ratio reinforced concrete walls", Engineering Structures, 32(2), 894-901.

[8] ATC-13, 1985, "Earthquake damage evaluation data for California, applied technology council. FEMA contract no. EMW-C-0912, Redwood City, CA.

[9] Rota, M., Penna, A., and Strobbia, C.L., 2008, "Processing Italian damage data to derive typological fragility curves", Journal of Soil Dynamic Earthquake Engineering, 28, 933-947.

[10] Bank, L.C., 2006, "Composites for construction: structural design with FRP materials", John Wiley and Sons, Inc., Hobboken, NJ.

[11] Bakis, C.E., Bank, L.C., Brown, V.L., Cosenza, E., Davalos, J.F., Lesko, J.J., Machida, A., Rizkalla, S.H., and Triantafillou, T.C., 2002, "Fiber-Reinforced Polymer Composites for Construction-State-of-the-Art Review", Journal of Composites for Construction, 6(2), 73-87.

[12] JMP, 2014, "JMP: statistical discovery: version 11", SAS Institute Inc., Cary, NC.

[13] Smith, S.T. and Teng, J.G., 2002, "FRP-strengthened RC beams. II: assessment of debonding strength models", Engineering Structures, 24, 397-417.

[14] Smith, S.T. and Teng, J.G., 2001, "Interfacial stresses in plated beams", Engineering Structures, 23(7), 857-871.

[15] BASF. 2007. MBrace® CF130 Unidirectional high strength carbon fiber fabric for the MBrace composite strengthening system, BASF Construction Chemicals, Shakopee, MN.

[16] Choi, E., 2002, "Seismic Analysis and Retrofit of Mid-America Bridges", PhD thesis, Georgia Institute of Technology, Atlanta, GA.

[17] Kim, Y.J., and Harries, K., 2013, "Statistical characterization of reinforced concrete beams strengthened with FRP sheets", Journal of Composites for Construction, 17(3), 357-370.

[18] The MathWorks, 2013, "MATLAB and Statistics Toolbox Release", The MathWorks, Inc., Natick, MA.

[19] Oracle, 2008, "Oracle Crystal Ball", Oracle Corp., Redwood Shores, CA.

[20] Ahmed, O. 2000. Strengthening of RC beams by means of externally bonded CFRP laminates- improved model for plate end shear, PhD Thesis, Department of Civil Engineering, Catholicke University of Leuven, Belgium.

[21] Aidoo, J., Harries, K.A., and Petrou, M.F. 2006. Full-scale experimental investigation of repair of reinforced concrete interstate bridge using CFRP materials, Journal of Bridge Engineering, 11(3), 350-358.

[22] Arduini, M., Nanni, A., and Romagnolo, M. 2004. Performance of one-way reinforced concrete slabs with externally bonded fiber-reinforced polymer strengthening, ACI Structural Journal, 101(2), 193-201.

[23] Beber, A.J., Filho, A.C., and Campagnolo, J.L. 2001. CFRP in the strengthening of reinforced concrete beams, Proceedings of International Conference on FRP Composites in Civil Engineering, 391-398.

[24] Brena, S.F., Bramblett, R.M., Wood, S.L., and Kreger, M.E. 2003. Increasing flexural capacity of reinforced concrete beams using carbon fiber-reinforced polymer composites, ACI Structural Journal, 100(1), 36-46.

[25] Ceroni, F. and Prota, A. 2001. Experimental behavior of RC beams strengthened by FRP sheets, Proceedings of International Conference on Composites in Constructions, 499-504.

[26] Chan, T.K. and Niall, M. 2001. Strengthening of one-way slabs using carbon fibre plates: the effect of preload, CSE Research Bulletin, No. 14, Nanyang Technology University, Singapore.

[27] Chicoine, T. 1997. Analyse et conception d'ancrages sur les pouters renforcees en flexion a l'aide des materiaux composites, M.A.Sc. thesis, Department de genie civil, Universite de Sherbrooke, Sherbrooke, QC, Canada.

[28] David, E., Djelal, C., Ragneau, E., and Bodin, F.B. 1999. Use of FRP to strengthen and repair RC beams: experimental study and numerical simulations, Proceedings of the 8th International Conference on Advanced Composites for Concrete Repair, London, UK.

[29] Dimande, A.O. 2003. Interface influence on the flexural strengthening of concrete structures with FRP systems, MS Thesis, FEUP, Oporto.

[30] Fang, T.Q. 2002. Study on U-shaped sheet behavior of anti-debonding in the concrete beam reinforced flexurally with FRP, Master's thesis, Tsinghua University, Tsinghua, China.

[31] Fanning, P.J. and Kelly, O. 2001. Ultimate response of RC beams strengthened with CFRP plates, Journal of Composites for Construction, 5(2), 122-127.

[32] Gao, B., Leung, W.H., Cheng, C.M., Kim, J.K., and Leung, C.K.Y. 2001. Effects of adhesive properties on strengthening of concrete beams with composite strips, Proceedings of International Conference on FRP Composites in Civil Engineering, 423-432.

[33] Garden, H.N. and Hollaway, L.C. 1998. An experimental study of the influence of plate end anchorage of carbon fibre composite plates used to strengthen reinforced concrete beams, Composite Structures, 42, 175-188.

[34] Garden, H.N., Hollaway, L.C., and Thorne, A.M. 1997. A preliminary evaluation of carbon fibre reinforced polymer plates for strengthening reinforced concrete members, Structures and Buildings, 122, 127-142.

[35] Garden, H.N., Auantrill, R.J., Hollaway, L.C., Thorne, A.M., and Parke, G.A.R. 1998. An experimental study of the anchorage length of carbon fibre composite plates used to strength reinforced concrete beams, Construction and Building Materials, 12, 203-219.

[36] Grace, N.F., Abdel-Sayed, G., and Ragheb, W.F. 2002. Strengthening of concrete beams using innovative ductile fiber-reinforced polymer fabric, ACI Structural Journal, 99(5), 692-700.

[37] Juvandes, L.F.P. 1999. Strengthening and rehabilitation of concrete structures using CFRP composites, PhD Thesis, FEUP, Oporto.

[38] Kaminska, M.E. and Kotynia, R. 2000. Experimental research on RC beams strengthened with CFRP strips, Report No. 9, Department of Concrete Structures, Technical University of Lodz, Poland.

[39] Kim, Y.J., Fam, A., Kong, A., and El-Hacha, R. 2005. Flexural strengthening of RC beams using steel reinforced polymer (SRP) composites, American Concrete Institute (ACI) Special Publication on Fiber Reinforced Polymer Reinforcement for Concrete Structures (SP-230), 1647-1664.

[40] Kotynia, R. and Kaminska, M.E. 2003. Ductility and failure mode of RC beams strengthened for flexure with CFRP, Report No. 13, Department of Concrete Structures, Technical University of Lodz, Poland.

[41] Matthys, S. 2000. Structural behaviour and design of concrete members strengthened with externally bonded FRP reinforcement, PhD thesis, University of Ghent, Ghent, Belgium.

[42] M'Bazaa, I. 1995. Reinforcement en flexion des pouters en beton arme a l'aide des lamelles en materiaux composites: optimization de la longueur des lamelles, M.A.Sc. thesis, Department de genie civil, Universite de Sherbrooke, Sherbrooke, QC, Canada.

[43] Nguyen, D.M., Chan, T.K., and Cheong, H.K. 2001. Brittle failure and bond development length of CFRP-concrete beams, Journal of Composites for Construction, 5(1), 12-17.

[44] Quantrill, R.J., Hollaway, L.C., and Thorne, A.M. 1996. Experimental and analytical investigation of FRP strengthened beam response: part I, Magazine of Concrete Research, 48, 177, 331-342.

[45] Quattlebaum, J., Harries, K.A., and Petrou, M.F. 2005. Comparison of three CFRP flexural retrofit systems under monotonic and fatigue loads, Journal of Bridge Engineering, 10(6), 731-740.

[46] Rahimi, H. and Hutchinson, A. 2001.Concrete beams strengthened with externally bonded FRP plates, Journal of Composites for Construction, 5(1), 44-56.

[47] Reeve, B.Z. 2005. Effect of adhesive stiffness and CFRP geometry on the behavior of externally bonded CFRP retrofit measures subject to monotonic loads, MS Thesis, Department of Civil and Environmental Engineering, University of Pittsburgh, Pittsburgh, PA.

[48] Ritchie, P.A., Thomas, D.A., Lu, L., and Connelly, G.M. 1991. External reinforcement of concrete beams using fiber reinforced plastics, ACI Structural Journal, 88(4), 490-500.

[49] Ross, C.A., Jerome, D.M., Tedesco, J.W., and Hughes, M.L. 1999. Strengthening of reinforced concrete beams with externally bonded composite laminates, ACI Structural Journal, 96(2), 212-220.

[50] Saadatmanesh, H. and Ehsani, M.R. 1991. RC beams strengthened with GFRP plates I: experimental study, Journal of Structural Engineering, 117(11), 3417-3433.

[51] Sharif, A., Al-Sulaimani, G.J., Basunbul, I.A., Baluch, M.H., and Ghaleb, B.N. 1994. Strengthening of initially loaded reinforced concrete beams using FRP plates, ACI Structural Journal, 91(2), 160-168.

[52] Shin, Y.S. and Lee, C. 2003. Flexural behavior of reinforced concrete beams strengthened with carbon fiber-reinforced polymer laminates at different levels of sustaining load, ACI Structural Journal, 100(2), 231-239.

[53] Spadea, G., Bencardino, F., and Swamy, R. 1998. Structural behavior of composite RC beams with externally bonded CFRP, Journal of Composites for Construction, 2(3), 132-137.

[54] Tan, K.H. and Mathivoli, M. 1999. Behaviour of preloaded reinforced concrete beams strengthened with carbon fibre sheets, 4th International Symposium on Fibre Reinforced Polymer for Reinforced Concrete Structures, Baltimore, MD, ACI-SP-188, 159-170.

[55] Teng, J.G., Smith, S.T., Yao, J., and Chen, J.F. 2003. Intermediate crack-induced debonding in RC beams and slabs, Construction and Building Materials, 17(6-7), 447-462.

[56] Triantafillou, T.C. and Plevris, N. 1992. Strengthening of RC beams with epoxy-bonded-fiber-composite materials, Materials and Structures, 25, 201-211.

[57] Tumialan, G., Serra, P., Nanni, A. and Belarbi, A. 1999. Concrete cover delamination in reinforced concrete beams strengthened with carbon fiber reinforced polymer sheets, ACI-SP 188, American Concrete Institute, Farmington, MI, 725-735.

[58] White, T.W., Soudki, K.A., and Erki, M.A. 2001. Response of RC beams strengthened with CFRP laminates and subjected to a high rate of loading, Journal of Composites for Construction, 5(3), 153-162.

[59] Xiong, G.J., Jiang, H., Huang, J.Z., Yang, J.Z., and Xie, H.C. 2001. Behavior of concrete beams strengthened with hybrid carbon fiber glass fiber sheets, Proceedings of International Conference on FRP Composites in Civil Engineering, 407-414.

[60] Ye, L.P., Cui, W., and Yue, Q.R. 2001. Analysis and calculation of flexural strength of RC members strengthened with CFRP sheet, Building Structures, 35(3), 3-5.

[61] Yi, W.J. and Huang, H.M. 2001. Experimental study on the flexural behavior of RC beams strengthened with CFRP laminates, Proceedings of International Conference on FRP Composites in Civil Engineering, 399-406.

[62] Zhao, M., Zhao, H.D., and Zhang, Y. 2002. Experimental study on flexural RC members strengthened with CFRP fabrics, Structural Engineering, 2, 52-58.

Table 1— Experimental database of FRP-strengthened beams partially reproduced based on [17]

Reference	Beam ID	h (mm)	w (mm)	L (mm)	f'_c (MPa)	ρ (%)	t_f (mm)	a (mm)
Ahmed [20]	AF.2	225	125	1500	41	0.36	0.33	500
	Af.2-1	225	125	1500	41	0.36	0.33	500
	AF.3	225	125	1500	41	0.36	0.33	500
	AF.4	225	125	1500	41	0.36	0.33	500
	DF.1	225	125	1500	42	0.54	0.17	500
	DF.2	225	125	1500	42	0.54	0.33	500
	DF.3	225	125	1500	40.5	0.54	0.5	500
	DF.4	225	125	1500	40.5	0.54	0.67	500
	BF.2-1	225	125	1500	41	0.36	0.33	500
	BF.3-1	225	125	1500	41	0.36	0.33	500
	CF.2-1	225	125	1500	43	0.46	0.33	500
	CF.3-1	225	125	1500	43	0.54	0.33	500
	CF.4-1	225	125	1500	43	0.74	0.33	500
	EF.1-1	225	125	1500	46	0.54	0.33	500
	EF.3-1	225	125	1500	38	0.54	0.33	500
	EF.4-1	225	125	1500	33	0.54	0.33	500
	FF.2-3	225	125	1500	39.5	0.54	0.5	700
Aidoo et al. [21]	CS	825	343	8840	45	2.62	1.4	4420

Reference	Beam ID	h (mm)	w (mm)	L (mm)	f'_c (MPa)	ρ (%)	t_f (mm)	a (mm)
Arduini et al. [22]	S-T1L1p	240	1500	4500	38.8	0.25	0.165	1500
	S-T2L1	240	1500	4500	38.8	0.78	0.165	1500
	S-T2L2	240	1500	4500	38.8	0.78	0.66	1500
	S-T3L1	240	900	4500	38.8	0.57	0.165	1500
	S-T3L2	240	1500	4500	38.8	0.34	0.165	1500
	S-T4L1	240	1500	4500	38.8	2.02	0.165	1500
	S-T4L2	240	1500	4500	38.8	2.02	0.33	1500
Beber et al. [23]	VR5	250	120	2349	33.6	0.52	0.44	783
	VR6	250	120	2349	33.6	0.52	0.44	783
	VR7	250	120	2349	33.6	0.52	0.77	783
	VR8	250	120	2349	33.6	0.52	0.77	783
	VR9	250	120	2349	33.6	0.52	1.1	783
	VR10	250	120	2349	33.6	0.52	1.1	783
Brena et al. [24]	A1	356	203	2690	35.1	0.56	0.33	1065
	A2	356	203	2690	35.1	0.56	0.33	1065
	A3	356	203	2690	35.1	0.56	0.33	1065
	A4	356	203	2690	37.2	0.56	0.165	1065
	B1	356	203	2690	37.2	0.56	0.336	1065
	B3	356	203	2690	37.2	0.56	0.336	1065
	C1	406	203	3000	35.1	0.49	2.08	1220
	C2	406	203	3000	35.1	0.49	2.08	1220
	C4	406	203	3000	37.2	0.49	2.08	1220
	D1	406	203	3000	37.2	0.49	1.19	1220
	D2	406	203	3000	37.2	0.49	1.19	1220
	D3	406	203	3000	37.2	0.49	2.38	1220
Ceroni & Prota [25]	A2	100	150	1800	29	0.67	0.165	750
	A3	100	150	1800	29	0.67	0.165	750
Chan & Niall [26]	S6-50-0	100	330	2500	53.36	0.34	1.2	850
	S6-50-1	100	330	2500	53.36	0.34	1.2	850
	S8-50-0	100	330	2500	53.36	0.61	1.2	850
	S8-50-1	100	330	2500	53.36	0.61	1.2	850
Chicoine [27]	P0	300	200	3000	44.3	0.26	0.9	1000
	P1	300	200	3000	44.3	0.26	0.9	1000
	P3	300	200	3000	44.3	0.26	0.9	1000
David et al [28]	P4	300	150	2800	40	0.68	6	900
	P7	300	150	2800	40	0.68	1.2	900
Dimande [29]	V.A	100	75	900	46.9	0.75	0.117	450
	V.B	100	75	900	46.9	0.75	0.117	450
	V.C	100	75	900	46.9	0.75	0.117	450
	V.D	100	75	900	46.9	0.75	0.117	450
	V.E	100	75	900	46.9	0.75	0.117	450
	V.F	100	75	900	46.9	0.75	0.351	450
	V.G	100	75	900	46.9	0.75	0.351	450
	V.H	100	75	900	46.9	0.75	1.4	450
Fang [30]	B1	200	150	1500	24.96	0.50	0.11	550
	B2	200	150	1500	24.96	0.50	0.11	550
	B3	200	150	1500	24.96	0.50	0.11	550
Fanning & Kelly [31]	F10	240	155	2800	80	0.91	1.2	1100
	F3	240	155	2800	80	0.91	1.2	1100
	F4	240	155	2800	80	0.91	1.2	1100
	F5	240	155	2800	80	0.91	1.2	1100
	F6	240	155	2800	80	0.91	1.2	1100
	F7	240	155	2800	80	0.91	1.2	1100
	F8	240	155	2800	80	0.91	1.2	1100
	F9	240	155	2800	80	0.91	1.2	1100
Gao et al. [32]	BB1	200	150	1500	35.7	0.52	0.22	500
	BB2	200	150	1500	35.7	0.52	0.22	500

Seo et al.

Reference	Beam ID	h (mm)	w (mm)	L (mm)	f'_c (MPa)	ρ (%)	t_f (mm)	a (mm)
	BB3	200	150	1500	35.7	0.52	0.22	500
	BB4	200	150	1500	35.7	0.52	0.44	500
	BB5	200	150	1500	35.7	0.52	0.44	500
	BB6	200	150	1500	35.7	0.52	0.44	500
Garden & Hollaway [33]	Can-05	100	100	1174	51.2	0.85	0.82	587
	Can-06	100	100	1544	51.2	0.85	0.82	772
	Can-07	100	100	1544	51.2	0.85	0.82	772
Garden et al [34]	1Au	100	100	900	57.9	0.85	0.5	300
	2Au	100	100	900	57.9	0.85	0.5	340
	3Au	100	100	900	57.9	0.85	0.5	400
	1Bu	100	100	900	57.9	0.85	0.7	300
	1B2u	100	100	900	57.9	0.85	0.7	300
	2Bu	100	100	900	57.9	0.85	0.7	340
	3Bu	100	100	900	57.9	0.85	0.7	400
	1Cu	100	100	900	57.9	0.85	1	300
	2Cu	100	100	900	57.9	0.85	1	340
	3Cu	100	100	900	57.9	0.85	1	400
Garden et al [35]	1U1.0	100	100	1000	44.8	0.85	0.82	300
	2U1.0	100	100	1000	44.8	0.85	0.82	300
	3U1.0	100	100	1000	44.8	0.85	0.82	340
	4U1.0	100	100	1000	44.8	0.85	0.82	400
	5U1.0	100	100	1000	44.8	0.85	0.82	400
	1U2.3	230	130	2300	39	0.79	0.82	845
	1U4.5	230	145	4500	39	0.68	0.82	1525
Grace et al. [36]	C-3	254	152	2440	55.2	1.04	1.9	839
Juvandes [37]	LA3R	76	441	1600	60.2	0.25	0.222	550
	LB1R	81	438	1600	61.6	0.24	0.222	550
	LC3R	81	425	1600	65.8	0.25	0.222	550
	LC4R	77	445	1600	65.5	0.25	0.222	550
	LA4S	80	435	1600	60.3	0.24	1.2	550
	LB2S	85	439	1600	61.8	0.23	1.2	550
	LC1S	81	439	1600	65.6	0.24	1.2	550
	LC2S	85	438	1600	65.7	0.23	1.2	550
	LD3BL	85	433	1600	49.2	0.23	1.4	550
	LD4BL	81	445	1600	49	0.24	1.4	550
	LE3I	82	437	1600	50.2	0.24	1.4	550
	LE4I	78	441	1600	50.2	0.25	1.4	550
	A.1	150	100	1500	31.6	1.05	1.2	650
	A.4	150	100	1500	38.4	1.05	1.2	650
	B.7	150	75	1500	36	0.13	1.2	650
	B.11	150	75	1500	32.4	0.13	1.2	650
	C.5	150	150	1410	21.3	2.01	1.2	605
Kaminska and Kotynia [38]	B-04/S	300	150	3000	28.5	0.35	1.2	800
	B-04/S L2.1	300	150	2100	28.5	0.35	1.2	800
	B-04/M	300	150	3000	29.7	0.35	1.2	800
	B-04/M L2.1	300	150	2100	29.7	0.35	1.2	800
	B-06/S	300	150	3000	32.3	0.50	1.2	800
	B-06/S	300	150	3000	32.3	0.50	1.2	800
	B-08/S	300	150	3000	33.8	0.75	1.2	800
	BO-08/S	300	150	3000	36.5	0.75	1.2	800
	BF-04/0.5S	300	150	3000	33	0.35	1.2	1500
	BF-06/S	300	150	3000	32.5	0.50	1.2	1500
Kim et al. [39]	SRP 30	150	100	1110	46.2	1.33	1.2	555
	SRP 60	150	100	1110	46.2	1.33	1.2	555

12

Reference	Beam ID	h (mm)	w (mm)	L (mm)	f'_c (MPa)	ρ (%)	t_f (mm)	a (mm)
	SRP 100	150	100	1110	46.2	1.33	1.2	555
Kotynia and Kaminska [40]	B-08M	300	150	4200	37.3	0.50	1.4	1400
	B-08Mk	300	150	4200	32	0.50	1.4	1400
	B-08Mn	300	150	4200	38.2	0.50	1.4	1400
	B-08S	300	150	4200	32.3	0.50	1.2	1400
	B-083m	300	150	4200	34.4	0.50	1.14	1400
	B-083mb	300	150	4200	25.8	0.50	0.76	1400
	BO-08Smb	300	150	4200	27.4	0.50	1.2	1400
Matthys [41]	BF2	450	200	3800	36.5	0.89	1.2	1250
	BF3	450	200	3800	34.9	0.89	1.2	1250
	BF4	450	200	3800	30.8	0.89	1.2	1250
	BF5	450	200	3800	37.4	0.89	1.2	1250
	BF8	450	200	3800	39.4	0.45	1.2	1250
	BF9	450	200	3800	33.7	0.45	1.2	1250
	B3	400	300	3800	30	0.33	0.51	1100
M'Bazaa [42]	P0	300	200	3000	44.3	0.33	0.9	1000
Ngyuen et al. [43]	A950	95	120	1500	32.1	2.07	1.2	250
	A1100	95	120	1500	32.1	2.07	1.2	250
	A1150	95	120	1500	32.1	2.07	1.2	250
	B1	93	120	1500	44.6	0.51	1.2	250
	B2	100	120	1500	44.6	5.24	1.2	250
	C5	135	120	1500	25.1	1.45	1.2	240
	C10	125	120	1500	25.1	1.57	1.2	240
	C20	105	120	1500	25.1	1.87	1.2	240
Quantrill et al. [44]	A1b	100	100	1000	58.1	0.85	1.2	300
	B2	100	100	1000	44	0.85	1.2	300
	B3	100	100	1000	44	0.85	1.2	300
	B4	100	100	1000	44	0.85	1.6	300
Quattlebaum et al. [45]	CS	254	152	4600	29.9	0.98	1.4	2300
Rahimi & Hutchinson [46]	A4	150	200	2100	54	0.52	0.8	750
	A5	150	200	2100	54	0.52	0.8	750
	A6	150	200	2100	54	0.52	1.2	750
	A7	150	200	2100	54	0.52	1.2	750
	A8	150	200	2100	54	0.52	0.8	750
	A9	150	200	2100	54	0.52	0.8	750
	B3	150	200	2100	54	0.52	0.4	750
	B4	150	200	2100	54	0.52	0.4	750
	B5	150	200	2100	54	0.52	1.2	750
	B6	150	200	2100	54	0.52	1.2	750
	B7	150	200	2100	54	0.52	1.8	750
	B8	150	200	2100	54	0.52	1.8	750
Reeve [47]	L1	250	150	4537	23.3	1.01	1.4	2268.5
	L2	250	150	4537	23.3	1.01	1.4	2268.5
	L2x1	250	150	4537	23.3	1.01	1.4	2268.5
	L4	250	150	4537	23.3	1.01	1.4	2268.5
	H1	250	150	4537	23.3	1.01	1.4	2268.5
	H2	250	150	4537	23.3	1.01	1.4	2268.5
	H2x1	250	150	4537	23.3	1.01	1.4	2268.5
	H4	250	150	4537	23.3	1.01	1.4	2268.5
Ritchie et al. [48]	C	305	152	2438	40	0.55	4.8	915
	D	305	152	2438	40	0.55	4.8	915
	G	305	152	2438	43.2	0.55	4.2	915
	I	305	152	2438	40	0.55	4.06	914
	M	305	152	2438	43.2	0.55	1.27	914
	F	304.8	152	2438	35	0.67	9.4	914.4
	L	304.8	152	2438	35	0.67	1.27	914.4

Seo et al.

Reference	Beam ID	h (mm)	w (mm)	L (mm)	f'c (MPa)	ρ (%)	tf (mm)	a (mm)
Ross et al. [49]	B1	200	200	2742	54.8	0.46	4.5	914
	B2	200	200	2742	54.8	0.83	4.5	914
	B3	200	200	2742	54.8	1.24	4.5	914
	B4	200	200	2742	54.8	1.83	4.5	914
	B5	200	200	2742	54.8	2.50	4.5	914
	B6	200	200	2742	54.8	3.30	4.5	914
Saadatmanesh and Ehsani [50]	B	455	205	4575	35	1.05	6	1982
	D	455	205	4575	35	1.05	6	1982
Sharif et al. [51]	P3	150	150	1180	37.7	0.70	3	393
	P2	150	150	1180	37.7	0.70	2	393
Shin & Lee [52]	R2O	250	150	2200	18	0.71	0.22	800
	R3O	250	150	2200	18	1.06	0.22	800
Spadea et al [53]	A1.1	300	140	4800	24.9	0.96	1.2	1800
	A3.1	300	140	4800	24.9	0.96	1.2	1800
Tan and Mathivoli [54]	A00	150	100	1800	28.6	1.05	0.22	600
	A15	150	100	1800	31.4	1.05	0.22	600
	A25	150	100	1800	29.7	1.05	0.22	600
	A40	150	100	1800	31.4	1.05	0.22	600
	A60	150	100	1800	28.6	1.05	0.22	600
	A75	150	100	1800	28.5	1.05	0.22	600
	A90	150	100	1800	30.1	1.05	0.22	600
Teng et al. [55]	GS1-I	151.2	302	2000	22.56	0.34	1.27	1000
	CS1-I	150.8	303	2000	21.44	0.34	0.165	1000
	CP1-I	150.5	301.5	2000	27.04	0.69	1.2	1000
	CP2-I	151.9	303.6	2000	37.68	0.68	1.2	1000
Triantafillou & Plevris [56]	B4	127	76	1220	43.58	0.39	0.65	458
	B5	127	76	1220	43.58	0.39	0.65	458
	B6	127	76	1220	43.58	0.39	0.9	458
	B7	127	76	1220	43.58	0.39	0.9	458
	B8	127	76	1220	43.58	0.39	1.9	458
Tumialan et al. [57]	A1	300	150	2130	50.6	1.76	0.165	1065
	A2	300	150	2130	50.6	1.76	0.33	1065
	A7	300	150	2130	50.6	1.76	0.33	1065
	C1	300	150	2130	50.6	1.76	0.165	1065
White et al. [58]	RA	300	150	2800	45.6	1.56	0.44	1000
	RB	300	150	2800	45.6	1.56	0.44	1000
Xiong et al. [59]	CF1	150	120	1800	15.68	1.26	0.11	600
	GF1	150	120	1800	15.68	1.26	0.08	600
	CF3	120	80	1200	15.68	2.36	0.11	400
Ye et al. [60]	BM0	200	400	3760	40.24	1.15	0.111	1380
Yi & Huang [61]	B 06	180	100	2000	32.64	0.84	0.22	700
	B 08	180	100	2000	34	0.84	0.33	700
Zhao et al. [62]	LL-3	250	150	1600	20.16	0.60	0.166	600
	LL-4	250	150	1600	33.12	0.60	0.166	600
	LL-5	250	150	1600	20.16	0.82	0.083	600

h = beam height; w = beam width; L = span length; a = shear span; f'_c = concrete strength in compression; ρ = steel reinforcement ratio; t_f = FRP thickness; a = shear span length

[1 mm = 0.0394 in; 1 MPa = 145.038 psi]

Table 2—Average property of RSM parameters

Parameter	Property
h	212.9 mm [8.4 in]
w	204.3 mm [8.0 in]
L	2301.4 mm [7.6 ft]
ρ	0.79%
a	856.2 mm [33.7 in]
$\sqrt{f_c^{'}}$	6.37
$\sqrt{t_f}$	0.95

Table 3—Statistical coefficients for RSM parameters

Parameter	Coefficient	Parameter	Coefficient	Parameter	Coefficient	Parameter	Coefficient
β_0	0.699981860	β_9	0.000003708	β_{18}	-0.000001620	β_{27}	-0.000003888
β_1	-0.000222101	β_{10}	-0.000000073	β_{19}	0.000394565	β_{28}	0.031525656
β_2	0.000875085	β_{11}	-0.001131978	β_{20}	-0.001042398	β_{29}	-0.047545024
β_3	-0.000075095	β_{12}	0.000000265	β_{21}	0.000000078	β_{30}	0.000000146
β_4	-0.030622844	β_{13}	-0.000004066	β_{22}	0.000131358	β_{31}	-0.000056777
β_5	0.000119648	β_{14}	0.000755277	β_{23}	-0.000000219	β_{32}	-0.000947194
β_6	0.086594988	β_{15}	-0.000000676	β_{24}	0.000043769	β_{33}	-0.004190976
β_7	-0.764317041	β_{16}	0.000000399	β_{25}	0.000474248	β_{34}	-0.055246108
β_8	-0.000001033	β_{17}	-0.000295394	β_{26}	-0.008112305	β_{35}	0.257868896

Table 4—Multivariate analysis of variance

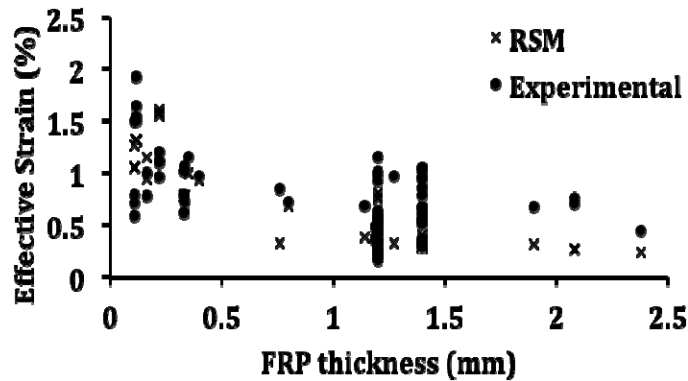| Parameter	F statistics	Significance
h	0.1763	0.6750
w	61.3873	<0.0001[*]
L	13.1175	0.0004[*]
ρ	3.46	0.0642
a	7.6919	0.0060[*]
$\sqrt{f_c^{'}}$	32.2942	<0.0001[*]
$\sqrt{t_f}$	391.2163	<0.0001[*]

[*]: statistically meaningful at a confidence level of 95%

[1 mm = 0.0394 in]

Fig. 1—Comparison between RSM and experimental effective strains with respect to FRP thickness

(a)

(b)

(c)

(d)

(e)

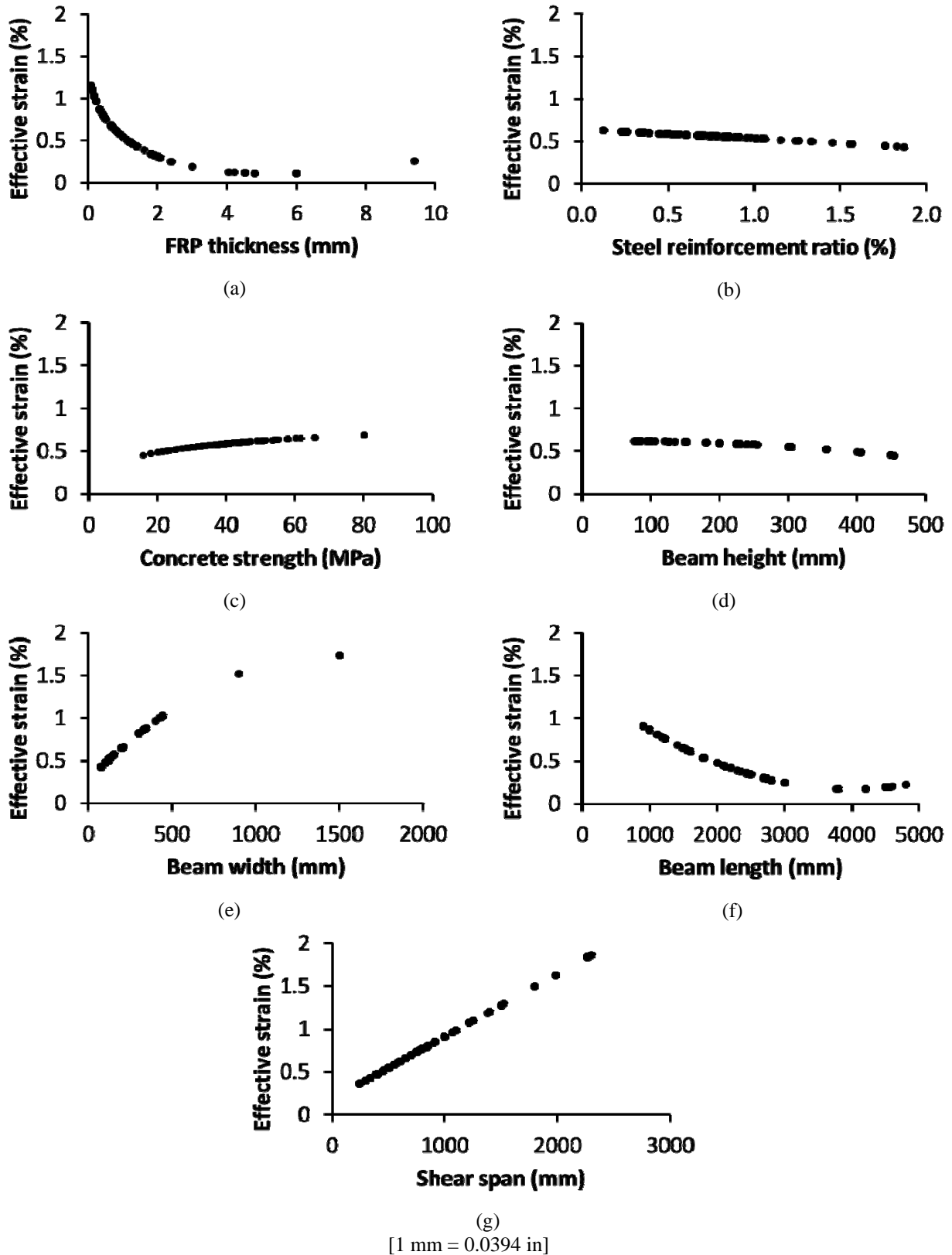(f)

(g)

[1 mm = 0.0394 in]

Fig. 2—Effect of single RSM parameters on effective strain of FRP-strengthened beams: (a) FRP thickness; (b) steel reinforcement ratio; (c) concrete strength; (d) beam height; (e) beam width; (f) beam length; (g) shear span
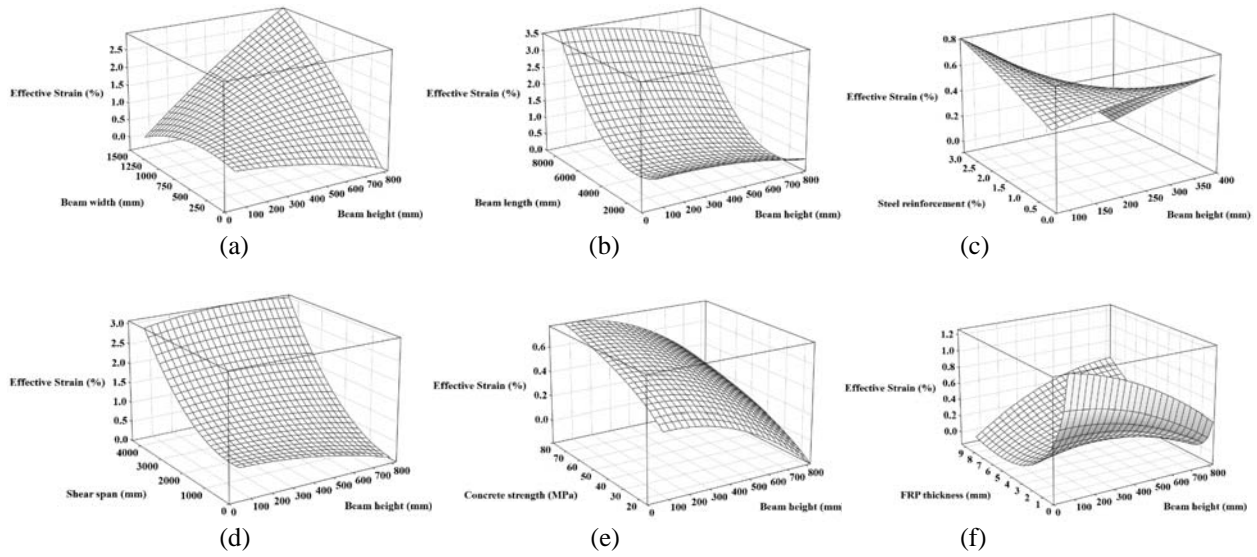
Fig. 3—Interaction between beam height and other parameters: (a) beam width; (b) beam length; (c) steel reinforcement ratio; (d) shear span; (e) concrete strength; (f) FRP thickness
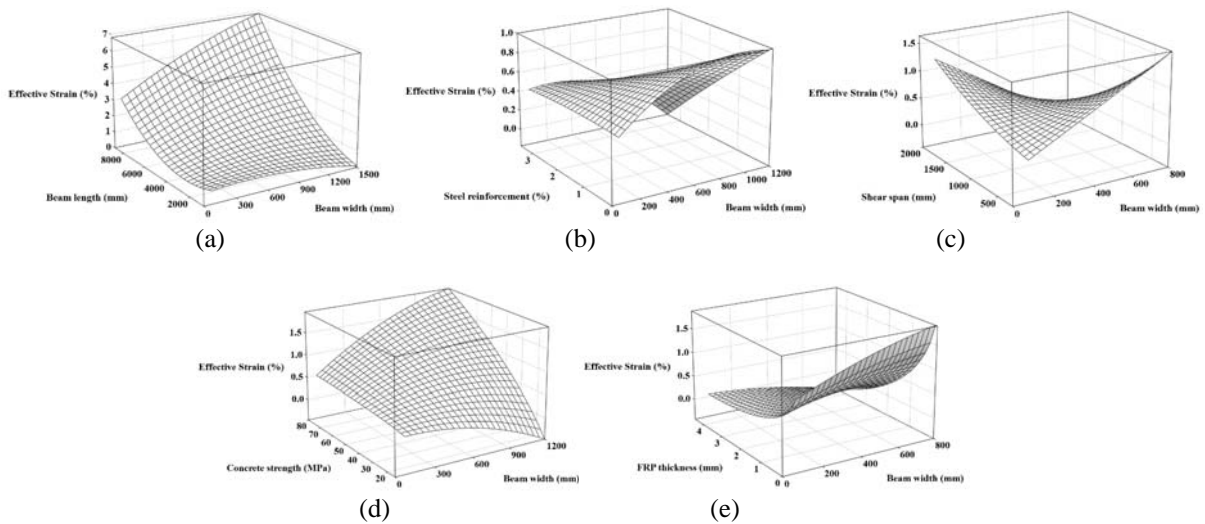

Fig. 4—Interaction between beam width and other parameters: (a) beam length; (b) steel reinforcement ratio; (c) shear span; (d) concrete strength; (e) FRP thickness
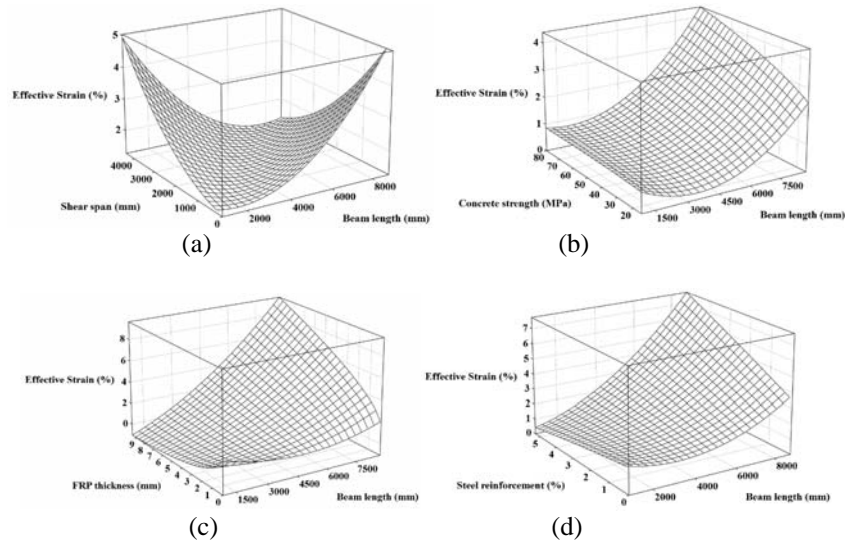
Fig. 5—Interaction between beam length and other parameters: (a) shear span; (b) concrete strength; (c) FRP thickness; (d) steel reinforcement ratio
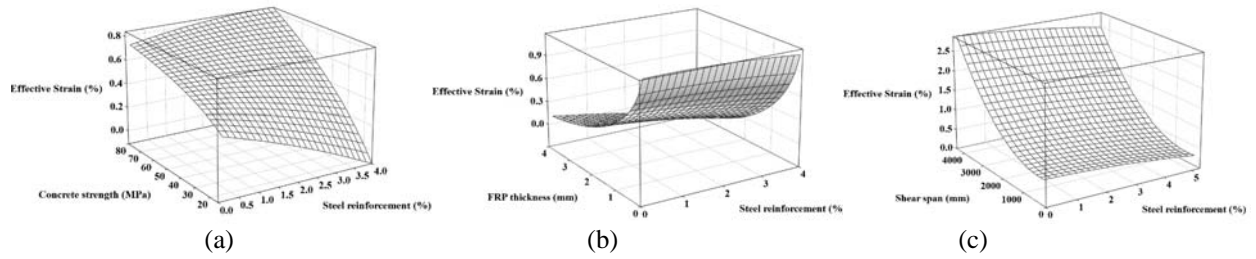
Fig. 6—Interaction between steel reinforcement ratio and other parameters: (a) concrete strength; (b) FRP thickness; (c) shear span
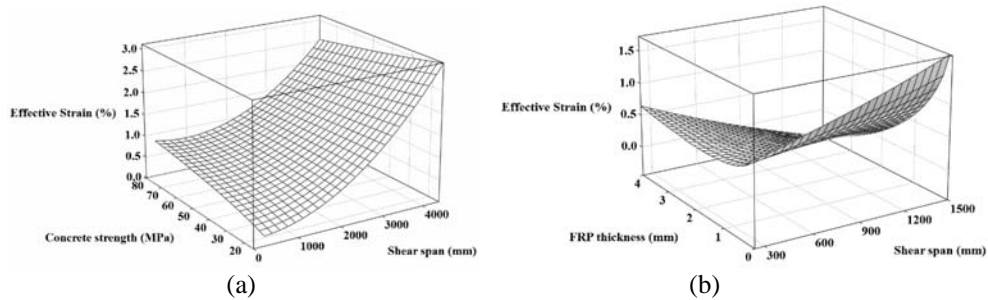
Fig. 7— Interaction between shear span and other parameters: (a) concrete strength; (b) FRP thickness
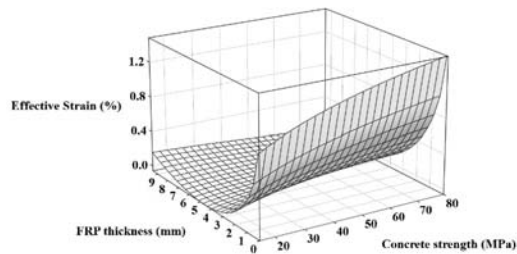

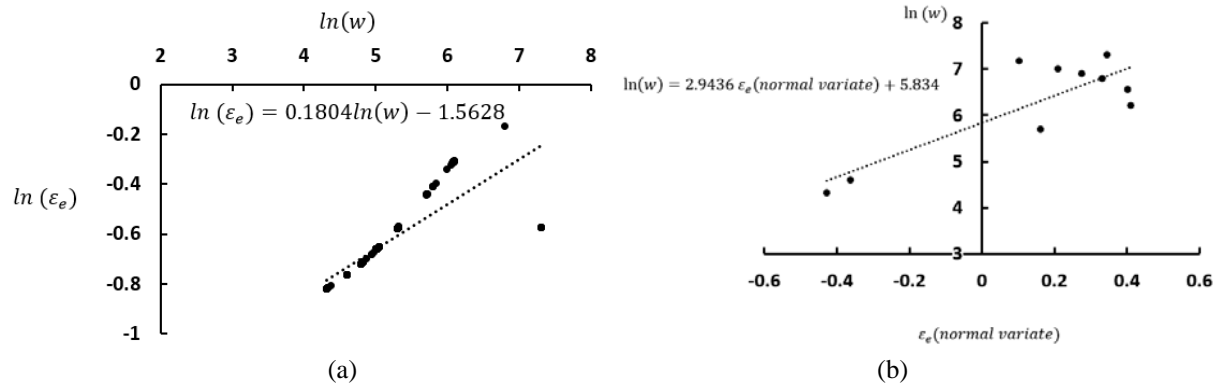
Fig. 8— Interaction between FRP thickness and concrete strength

Fig. 9—Log-normal probability plot of effective strain for a range of beam width: (a) conventional method; (b) joint RSM-MCS method

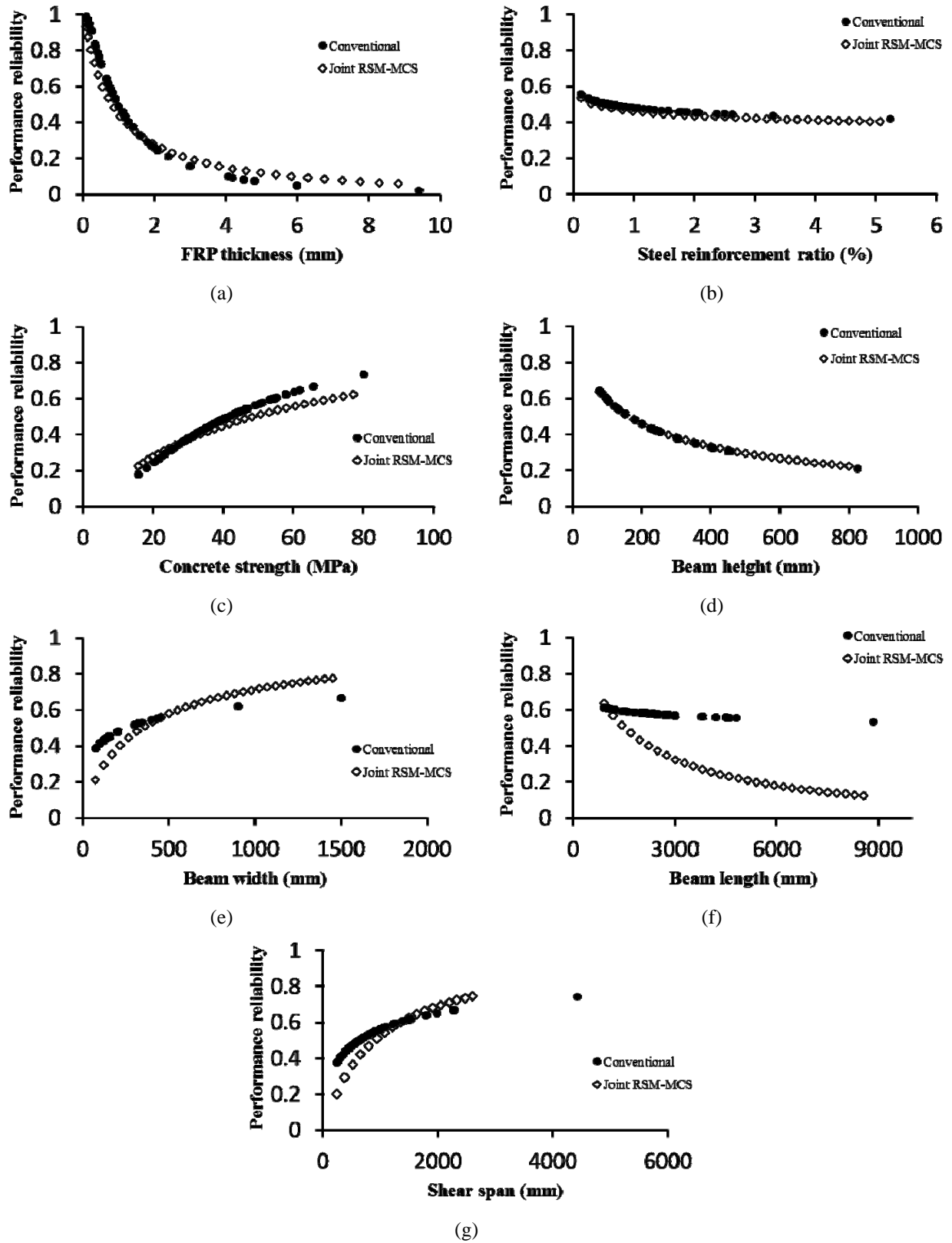Seo et al.

(a)

(b)

(c)

(d)

(e)

(f)

(g)

Fig. 10—Reliability response of FRP-strengthened beams: (a) FRP thickness; (b) steel reinforcement ratio; (c) concrete strength; (d) beam height; (e) beam width; (f) beam length; (g) shear span